

Dark Count Rate Stability of JUNO 20-inch PMTs in Mass Testing

Min Li^{a,b} Narongkiat Rodphai^{a,b} Caimei Liu^{a,b} Zhimin Wang^{a,b,1} Zhaoyuan Peng^{a,b} Jun Wang^e Nikolay Anfimov^f Denis Korablev^f Tobias Lachenmaier^c Alexander G. Olshevskiy^f Zhonghua Qin^a Tobias Sterr^c Alexander Felix Tietzsch^c Rong Zhao^e Wei Wang^e Kaile Wen^a Bjoern Soenke Wonsak^d Wan Xie^a Meihang Xu^a Yu Zhang^{a,b}

^a*Institute of High Energy Physics, Beijing 100049, China*

^b*University of Chinese Academy of Sciences, Beijing 100049, China*

^c*Eberhard Karls Universität Tübingen, Physikalisches Institut, Tübingen, Germany*

^d*Institute of Experimental Physics, University of Hamburg, Hamburg, Germany*

^e*Sun Yat-Sen University, Guangzhou, China*

^f*Joint Institute for Nuclear Research, Dubna, Russia*

E-mail: wangzhm@ihep.ac.cn

ABSTRACT: The Jiangmen Underground Neutrino Observatory (JUNO) is an ambitious multipurpose neutrino experiment designed to determine the neutrino mass ordering, with an impressive energy resolution goal of at least 3% at 1 MeV. To achieve a photon detection coverage of approximately 75%, JUNO will utilize two types of 20-inch photomultiplier tubes (PMTs): the large PMT (LPMT) and the microchannel plate PMT (MCP-PMT). A significant concern in high-precision neutrino measurements is the dark count rate (DCR) of PMTs, which introduces noise that can adversely affect energy measurement accuracy. During the mass testing phase of the JUNO 20-inch PMTs, comprehensive measurements of the DCR were undertaken. These measurements not only captured the DCR values of individual PMTs but also examined the stability and temperature dependence of the DCR at an operating gain of (1×10^7) . This paper presents a detailed characterization of the DCR of the JUNO 20-inch PMTs, investigating factors such as cooling time, temperature variations, and long-term stability using the JUNO Pan-Asia PMT testing facilities. The results reveal distinct DCR characteristics between the two types of PMTs, providing valuable insights into the nature of DCR and its implications for JUNO's scientific objectives. In addition to performance characterization, we implemented a monitoring system to track DCR stability over time. Notably, several spikes in DCR were identified, prompting a preliminary investigation into their causes. Potential factors contributing to these spikes, such as flasher events, were explored using coincidence rate analysis and complementary imaging techniques. The findings from this study are crucial for optimizing the performance of PMTs in JUNO, ultimately aiding the experiment in achieving its goals related to neutrino physics.

KEYWORDS: JUNO; 20-inch PMTs; DCR; Cooling Time; Temperature Effect; Flasher; Stability

¹Corresponding author.

Contents

1	Introduction	1
2	System Setup	2
2.1	20-inch Photomultiplier Tubes (PMTs)	2
2.2	Container System	3
3	Results and Discussions	4
3.1	DCR and Cooling Time	4
3.2	DCR and Temperature	7
3.2.1	Bare PMTs with Commercial Electronics	8
3.2.2	Potted PMT with 1F3 electronics	9
3.2.3	DCR and Room Temperature	12
3.3	DCR Spikes and Time	12
3.3.1	Long Stability of DCR	12
3.3.2	Short-term DCR Monitoring	16
3.4	Discussion	16
4	Possible Flasher Identification	17
4.1	DCR Spike	17
4.2	Investigation on DCR Spikes	18
4.2.1	Tagging with Artificial Spark	19
4.2.2	Check with Higher PMT HV	19
4.2.3	Discussion	20
5	Summary	20

1 Introduction

The Jiangmen Underground Neutrino Observatory (JUNO) [1, 2] is a multi-purpose neutrino experiment with the primary objective of precisely measuring the neutrino mass ordering at a significance level of $3\text{-}4\sigma$ within six years. The JUNO detector is strategically located approximately 53 km from both the Yangjiang and Taishan nuclear power plants. The detector comprises several sub-detectors, including the center detector (CD)[3], a veto detector featuring a water pool Cherenkov detector (WP), and a muon Top Tracker (TT). The CD is a liquid scintillator detector filled with 20 kton of liquid scintillator, which serves as the target. It will deploy a total of 17,612 20-inch photomultiplier tubes (LPMTs) [4] and 25,600 3-inch small photomultiplier tubes (SPMTs) [5] in pure water. This configuration aims to achieve an energy resolution of $3\%/\sqrt{E(\text{MeV})}$. In addition to the CD, another 2,400 LPMTs are employed in the WP to detect Cherenkov light produced by

cosmic muons. The PMT coverage is designed to exceed 78% (75% with LPMTs alone), aided by an average photon detection efficiency (PDE) exceeding 27%, which is essential for reaching the specified energy resolution. In total, JUNO will utilize 20,012 LPMTs, including 5,000 R12860-50 dynode-PMTs by Hamamatsu Photonics K.K. (HPK) and over 15,000 microchannel plate (MCP) PMTs from North Night Vision Technology Co., Ltd. (NNVT). These large-area PMTs have been successfully implemented in numerous large-scale particle physics experiments, including KamLand [6], Borexino [7], SNO [8], Super-Kamiokande [9], and Daya Bay [10], among others.

The large photomultiplier tubes (LPMTs) of the JUNO experiment will operate with a gain of (1×10^7) [11]. Extensive studies have been conducted on various parameters of these PMTs, including their timing characteristics, gain, and single-photon response.

Among the PMTs utilized, the 20-inch dynode PMT, model R12860-50 from Hamamatsu Photonics (HPK), has a dark count rate (DCR) that can be reduced to lower than 20 kHz [12]. Additionally, the newly developed 20-inch microchannel plate PMTs (MCP-PMT) from NNVT are anticipated to exhibit superior performance characteristics [13, 14].

To ensure thorough testing, all LPMTs for JUNO are evaluated using a specially designed mass testing system capable of assessing most relevant parameters [15–17]. This facility was located in Zhongshan City, Guangdong Province, China. The key characteristics of the LPMTs, including DCR, photon detection efficiency, and charge resolution, have been measured in line with JUNO’s requirements [4, 18, 19].

Given JUNO’s stringent energy resolution requirements, understanding and addressing the DCR of PMTs is vital for accurate energy measurement and reconstruction. The DCR is influenced by various sources, including thermionic emission from the photocathode and dynodes, leakage current, scintillation-induced photocurrents from the glass envelope or electrode supports, and ionization currents originating from residual gases. Moreover, gaining a comprehensive understanding of the DCR, alongside factors such as cooling time, temperature effects, and long-term stability, is essential for both the LPMTs and the JUNO experiment, beyond the traditional parameters evaluated in mass testing [4]. Flasher effects related to PMTs, which can lead to heightened DCR or substantial pulses in the PMTs, pose significant challenges for detectors designed for rare event detection [20–22]. Furthermore, large pulses generated from the PMT glass due to muon interactions and other radioactivities have been investigated in [23, 24]. Consequently, further exploration of potential flasher PMT candidates is valuable.

The layout of this paper is organized as follows: In Section 2, we will provide an overview of the LPMTs and the mass testing system. Section 3 will present and analyze the results, focusing on the DCR of the 20-inch PMTs with respect to cooling time and temperature effects. Section 4 will examine characteristics of potential flasher PMTs. Finally, a brief summary will be provided in Section 5.

2 System Setup

2.1 20-inch Photomultiplier Tubes (PMTs)

The JUNO experiment employs two types of 20-inch PMTs: approximately 5,000 box and linear-focused dynode PMTs (R12860-50 HQE or R12860) [25] from Hamamatsu Photonics (HPK),

and around 15,000 microchannel plate PMTs (MCP PMTs) (GDB-6201 or N6201) [26, 27], from North Night Vision Technology Co., Ltd. (NNVT). The selection of these PMTs was influenced by various factors, including performance parameters, costs, associated risks, and the overarching physics objectives of the JUNO project [28].

Designed to operate with a gain of (1×10^7) , the 20-inch PMTs in JUNO are subjected to a positive high voltage (HV) that takes into account considerations of cost, assembly, and noise. The detector is also designed to function within a temperature range of $(21 \pm 1 \text{ }^{\circ}\text{C})$ [29].

Both the DCR and PDE of the PMTs play critical roles in event reconstruction and have significant ramifications for physics measurements. The theoretical implications of the DCR for large liquid scintillator (LS) or water-based neutrino experiments have been discussed in the literature [28]. Extensive previous research has addressed various characteristics of DCR, as seen in studies such as [30–33]. For the PMTs accepted for JUNO, the mean DCR values are approximately 15.3 kHz for HPK PMTs and 49.3 kHz for NNVT PMTs, with a requisite cooling period of no less than 12 hours [4].

2.2 Container System

During the acceptance testing of JUNO, all 20-inch PMTs have been evaluated under several configurations. This includes testing bare PMTs with a plug-able high voltage (HV) divider for initial acceptance checks and water-proof potted PMTs paired with JUNO electronics.

The mass testing of these 20-inch PMTs was conducted using a container system (see Figure 1) [15] at the JUNO Pan-Asia testing and potting station in Zhongshan, China. Containers A and B are equipped with commercial electronics made by CAEN, located outside the containers, containing 36 individual channels (or drawers) each. Conversely, container D, which has 32 channels/drawer, is fitted with JUNO-designed electronics housed within, known as the 1F3 electronics (one electronics box servicing three PMT channels).

For DCR measurements, containers A and B employ a discriminator and scalar to count PMT pulses at a threshold of $3 \pm 1 \text{ mV}$ (around 0.3 p.e.). In contrast, container D utilizes the 1F3 electronics to measure DCR with a more precise threshold of $2 \pm 0.1 \text{ mV}$ (around 0.25 p.e.) [19]. The DCR is calculated by counting the PMT pulses over a 30-second interval, with results automatically retrieved by the data acquisition system based on the specified configuration.

To maintain stable testing conditions, the containers are equipped with a high-power HVAC (heating, ventilation, and air conditioning) system, which regulates the internal temperature to within $1 \text{ }^{\circ}\text{C}$ across a range of $-20 \text{ }^{\circ}\text{C}$ to $+45 \text{ }^{\circ}\text{C}$. Temperature sensors monitor all channels, with periodic readings taken every 60 seconds, achieving an accuracy of $0.25 \text{ }^{\circ}\text{C}$. During routine PMT tests, only container D operates under controlled conditions at $22 \text{ }^{\circ}\text{C}$ to ensure that the 1F3 electronics function in an environment similar to that of the JUNO detector, as they generate approximately 10 W of heat per channel. Containers A and B, however, are mostly operated without the HVAC and are subject to the ambient conditions of the warehouse, typically averaging $25 \text{ }^{\circ}\text{C}$ (with fluctuations between $22 \text{ }^{\circ}\text{C}$ to $26 \text{ }^{\circ}\text{C}$).

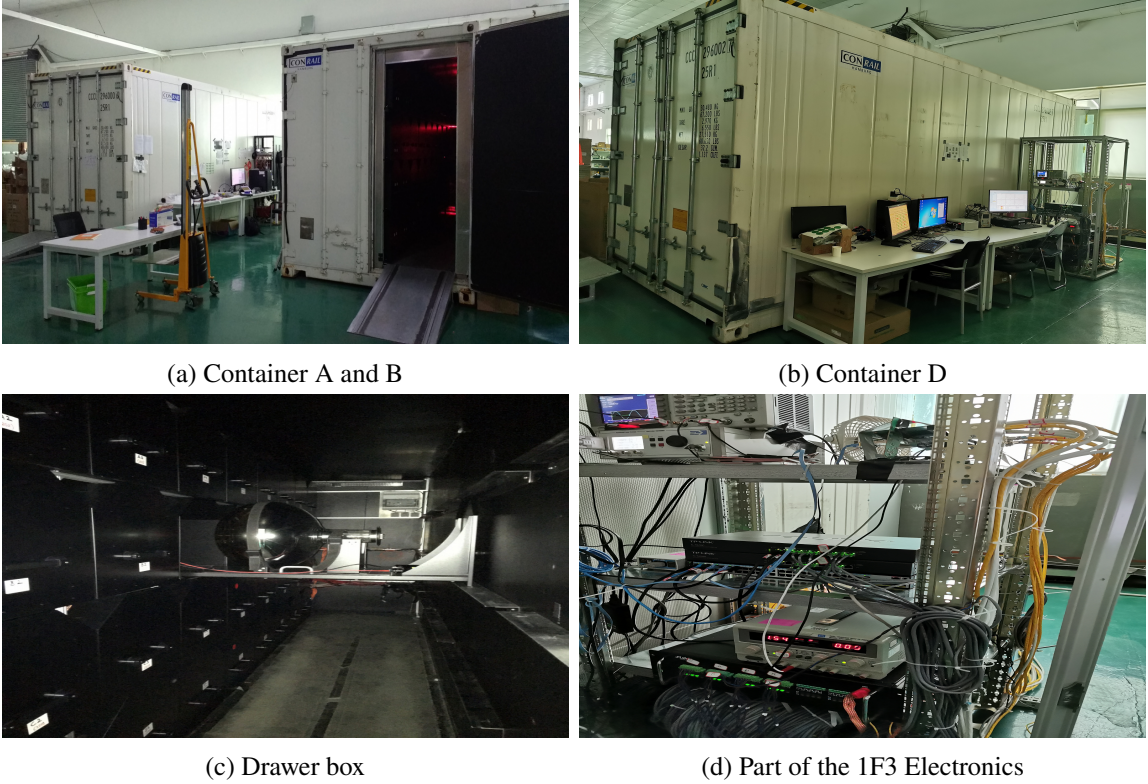


Figure 1: Container system

3 Results and Discussions

It is well established that the measured DCR is influenced by several factors, including cooling time, environmental conditions, and system gain. The long-term stability of the DCR is crucial for ensuring stable operation. This study aims to comprehensively address the various effects of DCR within the context of the container system.

3.1 DCR and Cooling Time

According to the standard procedure for JUNO PMT testing, it is inevitable that the PMT is exposed to light, even in dim conditions, during the loading and unloading processes. This exposure temporarily increases the measured DCR of the PMT, leading to the necessity of a cooling period to ensure accurate DCR measurement.

The relationship between the DCR and the cooling time of potted 20-inch PMTs is illustrated in Figure 2. The monitoring period for the DCR spans approximately 50 hours after the PMTs have been loaded and the high voltage (HV) has been applied. During this time, all PMTs are subjected to a comparable light intensity. The monitored DCR for each PMT is represented in distinct colors in Figure 2a (NNVT) and Figure 2b (HPK). Notably, the initial DCR of most NNVT PMTs is higher than HPK PMTs, which is likely due to the difference in the internal characteristics of the PMTs. The DCR of HPK PMTs stabilizes rapidly, whereas the DCR values among NNVT PMTs exhibit substantial variability. A minimum cooling period of 12 hours is implemented before DCR

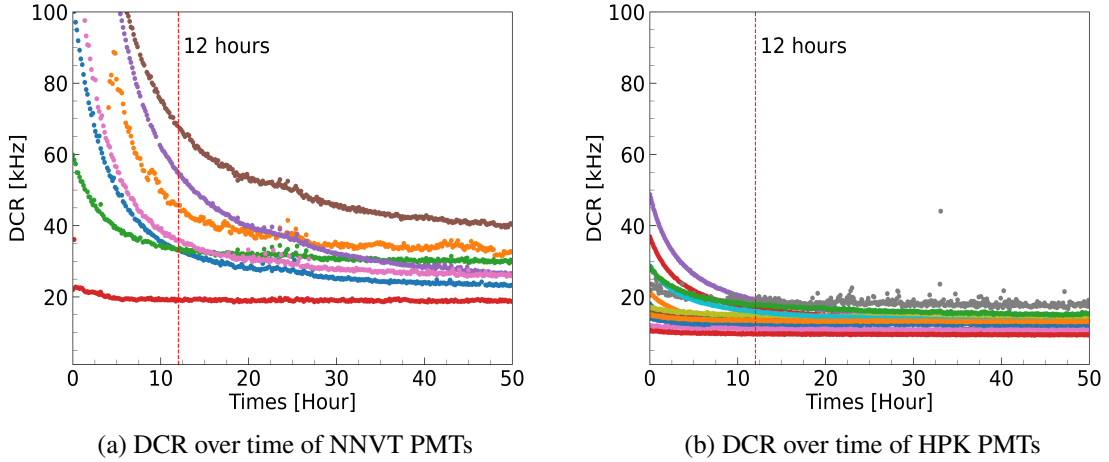


Figure 2: DCR and cooling time

measurement to facilitate an accurate assessment, while also considering preliminary monitoring and operational time constraints. Furthermore, gaining additional insights into the cooling characteristics of each PMT type could enhance predictions of the DCR over time.

The DCR variation ratio is defined based on the tested samples of each PMT type, as illustrated in Figure 3a. This ratio is normalized to the measurement taken at 12th hour. Both types of PMTs exhibited a rapid decline during the initial 12 hours; however, the rate of decrease slowed after this period.

To analyze the ratio plot shown in Figure 3a, we applied a fitting function described by:

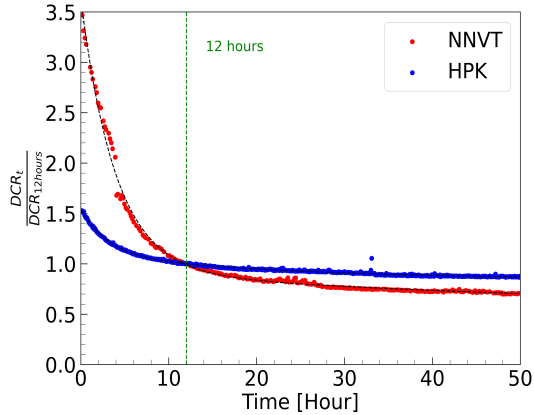
$$y = \frac{a_1}{\tau_1} \cdot e^{-\frac{x}{\tau_1}} + \frac{a_2}{\tau_2} \cdot e^{-\frac{x}{\tau_2}} + c \quad (3.1)$$

The fitting function 3.1 contains two components which represent the cooling factors, light exposure, and thermal effects. The results of this analysis are summarized in Table 1. The parameters a_1 and a_2 indicate the contributions of the respective components associated with τ_1 and τ_2 . Notably, the component associated with τ_1 has a more significant impact than that of τ_2 . The parameter c denotes the expected DCR when the cooling time is sufficiently extended, though its value is influenced by the specific test sample and the statistics recorded in Table 1.

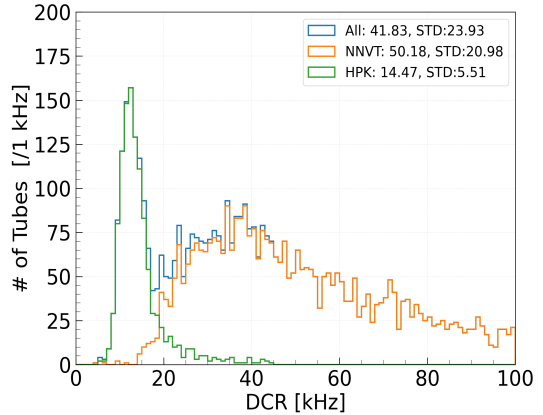
After 12 hours, the equation 3.1 related to the rapid factor τ_1 (approximately 3-4 hours) has nearly diminished. Additionally, it can be observed that the DCR of the potted NNVT PMT appears to require a longer time (52 hours) to attain a stable status compared to the potted HPK PMTs, which reach stability in 25 hours.

The ideal DCR of the measured PMTs is determined as a fraction of the DCR measured after 12 hours of cooling time. For NNVT tubes, the ideal DCR corresponds to 56% of the measured DCR after cooling, while for HPK tubes, it corresponds to 83% of the measured DCR after the same cooling period.

In the additional to the 12 hours DCR measurement, the DCR also was measured after 16



(a) Normalized DCR and time



(b) DCR of 20-inch PMTs at 12 hours

Figure 3: DCR test results in Pan-Asia

Table 1: Parameter distribution of time effect of potted PMTs

func.	a_1	τ_1	a_2	τ_2	c
HPK	1.42	3.11	6.30	24.99	0.83
NNVT	10.52	3.93	20.19	51.74	0.56

hours, which other parameters and the PDE also were analyzed during this measurement as well. However, since the measurement of these parameters included the use of a light source operated in the single photon regime, an increase of the in DCR in the second measurement was observed. Specifically, the increase in DCR for the NNVT is approximately $5 \pm 2\%$, while for the HPK, it is about $34 \pm 3\%$. A comparison between the two measurements at 12 hours can be seen in Figure 4.

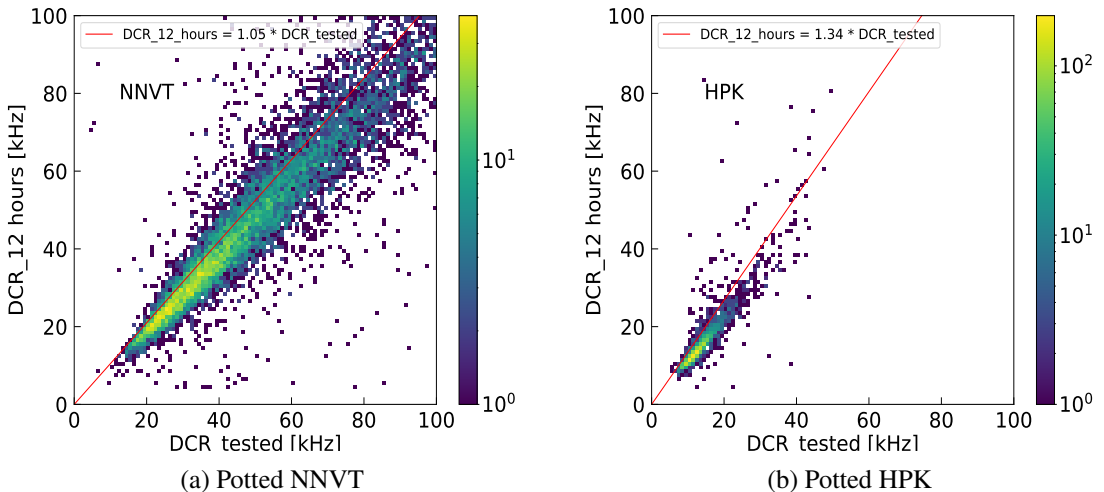


Figure 4: DCR comparison between potted NNVT and HPK PMTs, which the rates at 12h are in general higher than the rates at "tested"

Moreover, the DCR between bare and potted PMTs also was measured and analyzed, which observed a DCR decreasing after PMT's waterproof potting. This PMT's waterproof process indicates a significant difference between the behavior of NNVT and HPK PMTs under similar conditions. For the NNVT PMTs, the average DCR was reduced at least 60% to 31 ± 2 kHz, by tested PMTs after potting with containers A and B. This decrease suggests that the waterproof potting may be effectively mitigating certain noise contributions, associated with the bare NNVT PMTs. In contrast, the HPK PMTs exhibited stability in their mean DCR value, indicating that their design or materials might be inherently less susceptible to the noise factors which affected the NNVT PMTs. The general result of this comparison can be found in Figure 5.

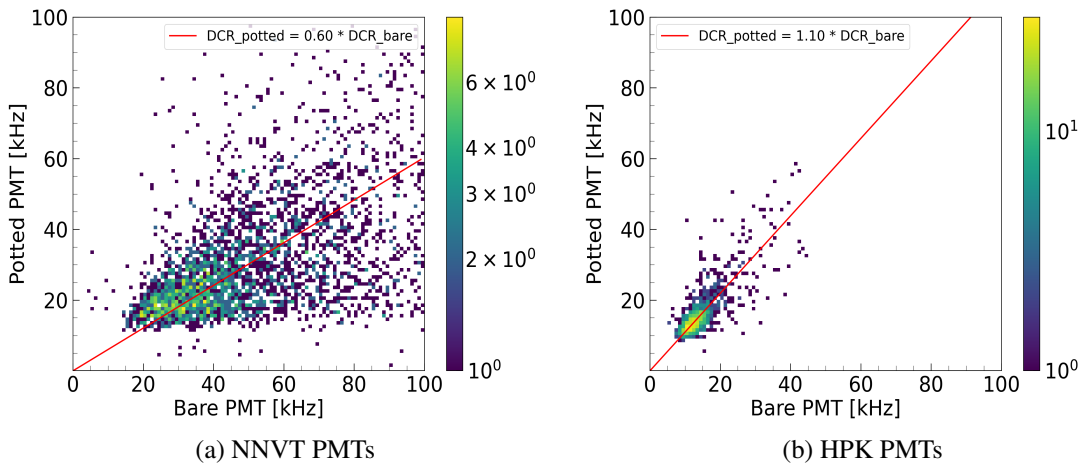


Figure 5: DCR comparison between bare and potted PMTs

3.2 DCR and Temperature

The temperature effect on the DCR was investigated after accounting for the cooling time effect. The study included three measurements including:

- Bare PMTs in Container B: Tagged as commercial electronics, this setup included two separate measurements—one with NNVT PMTs and another with HPK PMTs.
- Potted PMTs in Container D: Tagged as 1F3 electronics, measurements were conducted simultaneously using different types of PMTs.
- Room Temperature Variations in Container A: This setup, also tagged as commercial electronics, investigated the relationship between DCR and variations in room temperature.

Note that all measurements incorporated both NNVT and HPK PMTs.

During the experiment, the HVAC system of the container was used to manage the temperature inside the containers. The system was designed to maintain a temperature gradient of less than 2 $^{\circ}\text{C}$ per hour within a thermal range of 14 $^{\circ}\text{C}$ to 28 $^{\circ}\text{C}$. Although the monitored temperature of each drawer adjusted rapidly in response to the set points, it was ensured that the temperature

remained stable for an additional 2-3 hours at each set point, allowing the PMTs to achieve thermal equilibrium.

For the analysis of the relation between DCR and room temperature, we conducted a detailed review of long-term monitoring data. This was compared against measurements taken during short-term temperature surveys to assess the consistent effects of temperature variation of the DCR.

3.2.1 Bare PMTs with Commercial Electronics

The bare NNVT and HPK tubes were tested at different temperatures in two separate batches. This section will discuss each aspect individually.

- Heating and Cooling of NNVT PMTs

The results of the bare NNVT PMTs are presented in Figure 6, illustrating the heating and cooling processes. The monitored temperature, as depicted in Figure 6a, indicates that a waiting time of 2-3 hours is required for thermal equilibrium at each set point. The DCR observed during the heating and cooling phases is shown separately in Figure 6b and Figure 6c.

To facilitate comparison, the DCR curve for each PMT was normalized to its DCR value at 21 °C and averaged across all samples, as represented in Figure 6d. From this analysis, it can be concluded that the PMTs exhibit a similar trend during both heating and cooling processes. The maximum and minimum values of DCR variation are marked for each process.

For the bare NNVT PMTs, the average DCR variation is approximately 12%/°C within the measured temperature range, equating to an absolute change of about 6 kHz/°C (as summarized in Table 2). Notably, the variation in DCR during the heating process is smoother compared to the cooling process. This suggests that the PMTs require more time to achieve thermal equilibrium while cooling, particularly at the highest temperature (~27°C) observed.

- Heating and cooling of HPK PMTs

A similar measurement was conducted with bare HPK PMTs following the same procedures used for bare NNVT PMTs. The results are presented in Figure 7. Figure 7a, showing the monitored temperature during the cooling and heating phases, while Figure 7b and Figure 7c display the monitored DCR as a function of temperature for the two processes, respectively.

In the measured temperature range, the variation of the DCR with respect to temperature is only 1.5%/°C and approximately 0.2 kHz/°C, respectively, as shown in Figure 7d. In comparison to the bare NNVT PMTs, this variation is much smaller, indicating a more pronounced temperature effect on NNVT PMTs. The detailed results are also summarized in Table 2.

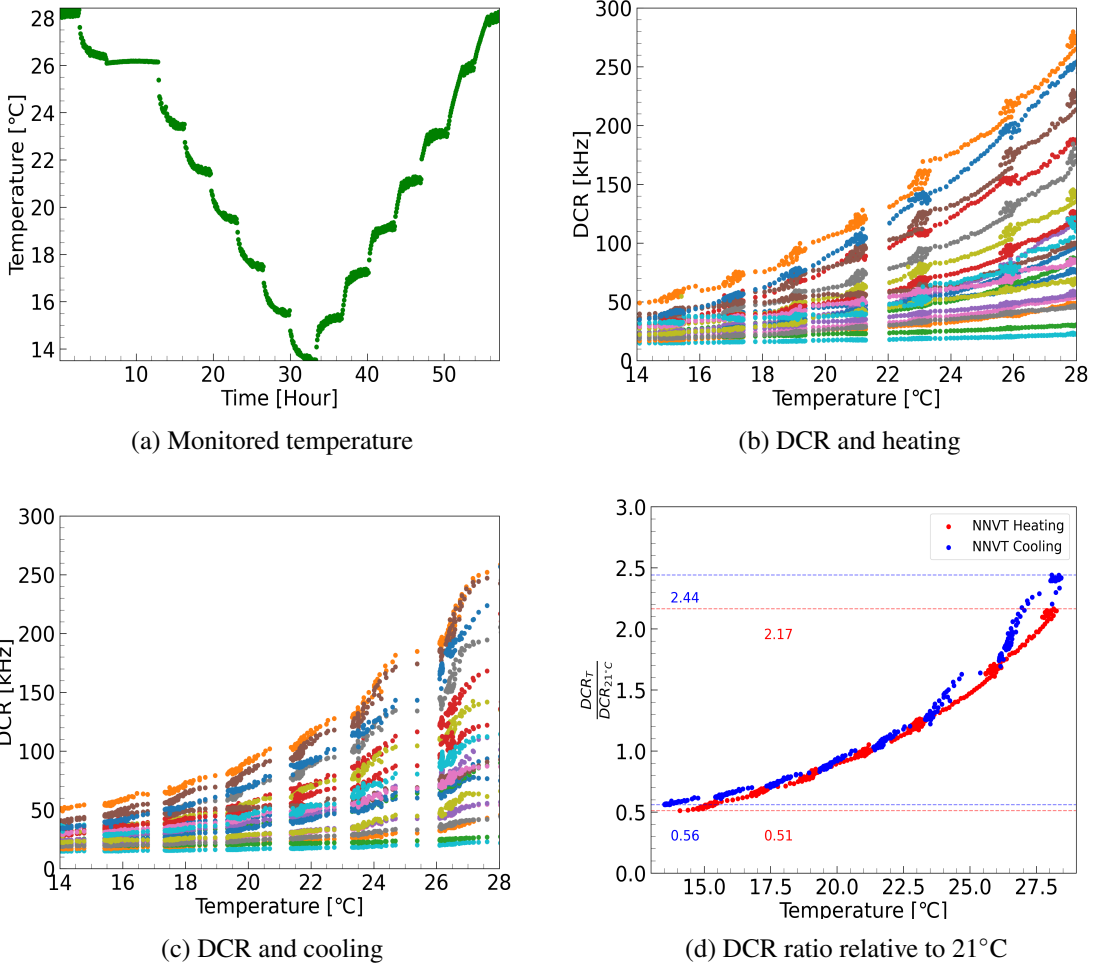


Figure 6: DCR and heating and cooling of bare NNVT PMTs, where the temperature is measured inside the drawers aside the PMT as discussed in section.2

Table 2: Parameters of temperature effect for bare PMTs

PMT		DCR/DCR_21 °C		Variation Ratio [%/°C]	DCR [kHz/°C]
		max.	min.		
HPK	heating	1.17	0.95	1.60	0.24
	cooling	1.13	0.95	1.43	0.22
NNVT	heating	2.17	0.51	11.67	6.23
	cooling	2.44	0.56	12.60	6.06

3.2.2 Potted PMT with 1F3 electronics

A series of tests on the potted NNVT and HPK PMTs have been conducted, using the 1F3 electronics housing within container D. These tests included a total of 11 HPK PMTs and 15 NNVT PMTs. The temperature was initially raised to 28 °C, which was the starting temperature of the monitoring of the DCR during the subsequent cooling process. To guarantee thermal equilibrium of the PMTs,

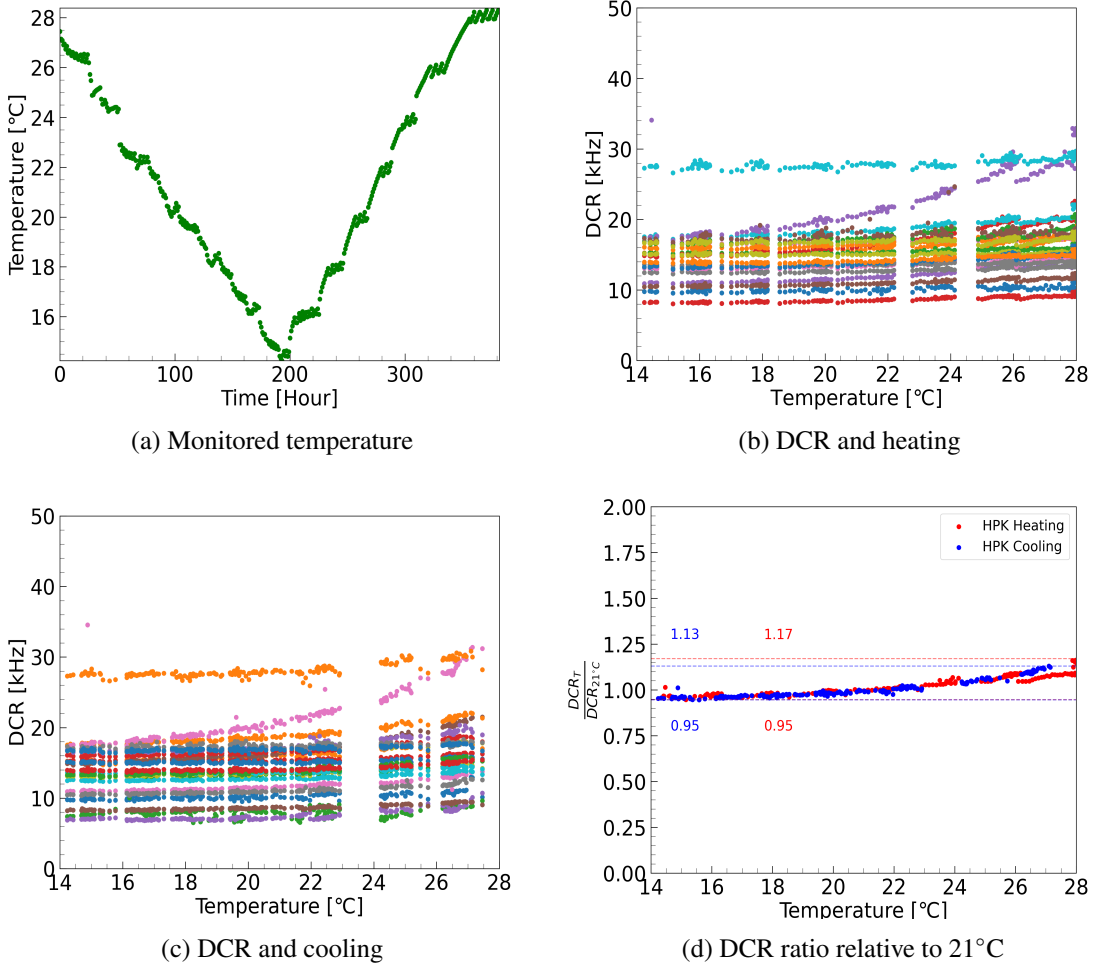


Figure 7: DCR and heating and cooling of bare HPK PMTs, where the monitored temperature is measured by sensors inside each drawers aside the PMT as discussed in section 2

a slow cooling rate of 1 °C every 2 hours was chosen.

Figure 8a illustrates the monitored temperature throughout the measurements, showing a cooling range from 28.3 °C to 14.6 °C, and a subsequent heating range from 14.6 °C back to 28.3 °C.

Figure 8b and 8c display the absolute DCR measured during the heating and cooling processes, respectively. Additionally, Figure 8d presents the normalized DCR ratio of each PMT compared to their DCR at 21 °C, along with the average of all samples. The highest and lowest ratio are indicated by dashed lines.

In summary, as shown in Table 3, the behavior of the potted NNVT and HPK PMTs mirrors that of the bare PMTs during the heating and cooling processes, but with reduced factors. The potted HPK PMTs exhibited a temperature coefficient of approximately 2%/°C, which aligns with the behavior of bare HPK PMTs. In contrast, the potted NNVT PMTs displayed a coefficient of around 4%/°C within the temperature range of 14 °C to 28 °C, notably lower than the bare NNVT

PMTs. This disparity might be due to two reasons: 1.) the trend in the temperature range of 14 °C to 21 °C is more stable. 2.) the waiting time for the PMTs to reach thermal equilibrium was shorter in the range of 14 °C to 21 °C. Additionally, the potting appears to contribute to a reduced DCR for the NNVT PMTs, as highlighted in Figure 5.

The parameters gathered from the DCR and temperature tests for the two separate batches of PMTs are summarized in Table 3, demonstrating consistent results across both measurements.

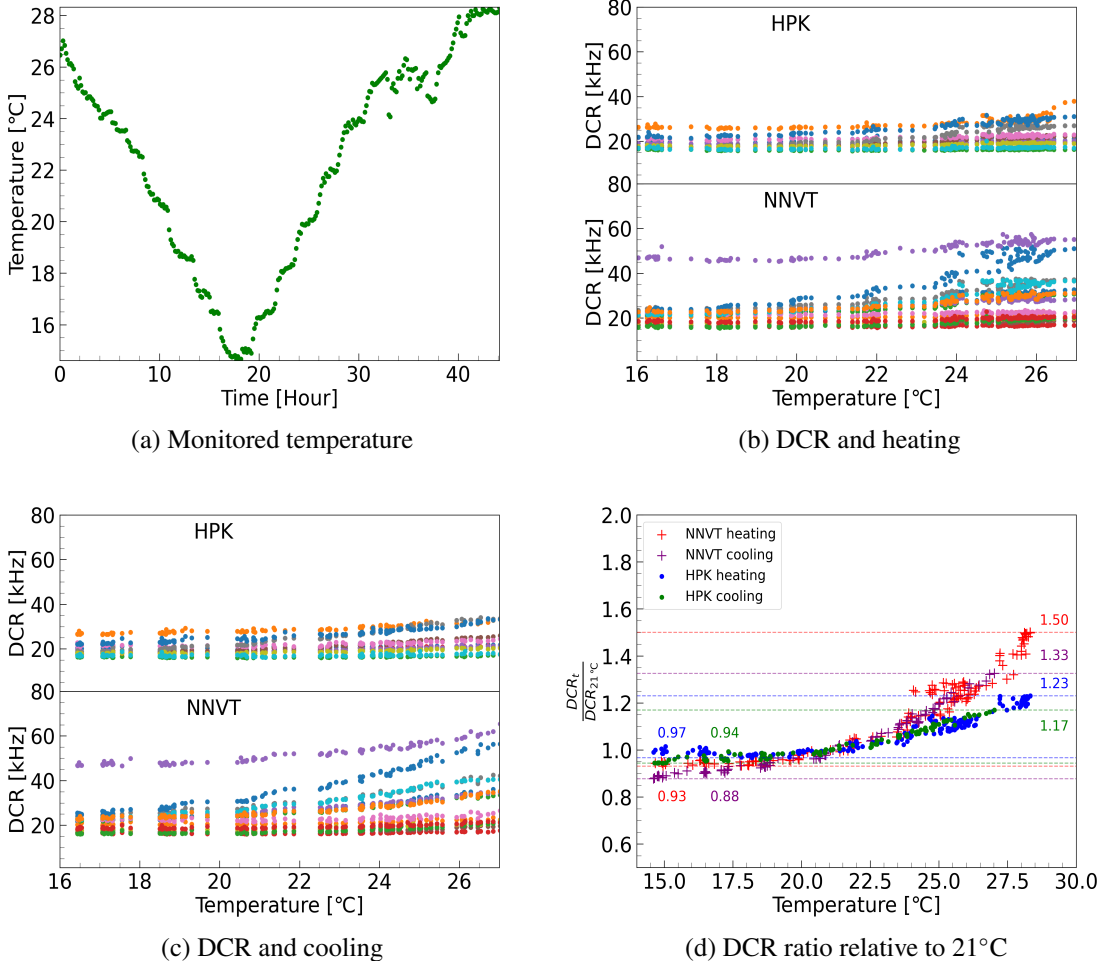


Figure 8: DCR and heating and cooling process of potted HPK and NNVT PMTs

Table 3: Parameters of DCR and temperature of potted PMTs

PMT		run 2537				run 2561			
		max.	min.	variation [%/°C]	abs.change [kHz/°C]	max.	min.	variation [%/°C]	abs.change [kHz/°C]
HPK	heating	1.23	0.93	1.92	0.37	1.22	0.97	2.00	0.41
	cooling	1.17	0.88	1.82	0.36	1.21	0.96	2.04	0.43
NNVT	heating	1.50	0.97	3.61	0.90	1.42	0.90	3.61	0.76
	cooling	1.33	0.94	4.17	0.83	1.39	0.94	4.12	0.90

3.2.3 DCR and Room Temperature

During PMT mass testing, the time duration of the PMTs occupied inside the container system was intentionally extended to assess how they responded across various temperature fluctuations around room temperature. In the analysis at hand, data set spanning 250 hours was examined. The monitored DCR during this test is illustrated in Figure 9. The average DCR measurements, aggregated from 6 potted NNVT PMTs and 12 potted HPK PMTs, are displayed alongside the temperature data in Figure 9a (NNVT PMTs) and Figure 9b (HPK PMTs).

The observations can be categorized into four distinct stages: two heating phases (Heating 1 and Heating 2) and two cooling phases (Cooling 1 and Cooling 2), all occurring within a temperature range of 24 °C to 26 °C. The average absolute DCR across the tested samples in relation to temperature is presented in Figure 9c and Figure 9d for each respective stage. The temperature variation inside during four stages are displayed in Figure 9e and 9f for both PMT types.

The rate of temperature change was quite gradual, ranging from -0.25 °C/hour to 0.25 °C/hour. For the HPK PMTs, all stages exhibited a consistent trend, with an average variation factor of 0.35 kHz/°C. However, in the cooling 1 stage, a deviation was noted, primarily attributed to insufficient cooling time following the loading of PMTs into the containers, as discussed in Section 3.1.

Similarly, for the NNVT PMTs, the trend remained consistent across all stages, with an average variation factor of 6.01 kHz/°C within the 24 °C to 26 °C range. Notably, the heating 2 stage displayed a sub-structure correlated to the temperature increase, particularly around 26 °C. This can likely be traced back to the rapid temperature change and the heightened sensitivity of NNVT PMTs to temperature variations.

Both short-term and long-term assessments confirm the consistency of performance among the potted PMTs throughout the heating and cooling processes within the specified temperature range.

3.3 DCR Spikes and Time

3.3.1 Long Stability of DCR

The long-term stability of the DCR is crucial for ensuring stable detector operation and accurate measurements. For JUNO experiment, fluctuations in the DCR during detector operation can lead to false triggers, thereby affecting the energy measurement accuracy [34–36].

To assess the stability of the DCR over time, various loads and runs of PMTs were conducted during the Pan-Asia testing, monitoring DCR stability for approximately 1000 hours. This is depicted in Figure 10, where the bare PMTs' performance is illustrated. The different colors in the background correspond to distinct periods during which the same PMTs were placed in various container channels.

Further analysis of the PMTs in container A, without temperature control, are shown in Figure 10a and Figure 10b. In contrast, Figs. 10c and 10d present results from PMTs in container D, which were tested under temperature control inside. The data indicates that NNVT PMTs exhibit more significant variations linked to temperature changes compared to HPK PMTs. This observation can primarily be attributed to the temperature effects, as discussed in Section 3.2.3.

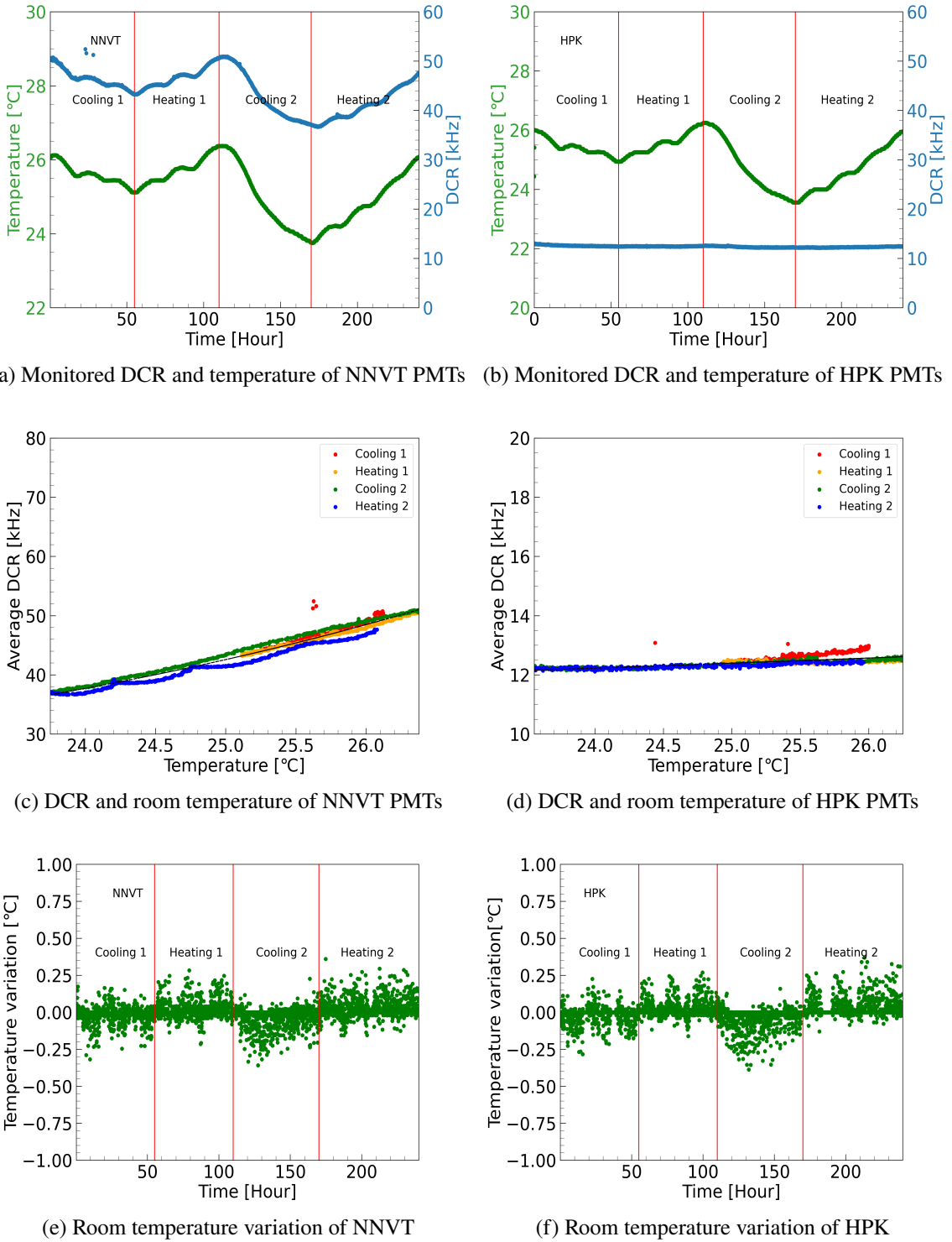


Figure 9: DCR and room temperature variation

This study highlights the importance of maintaining stable DCR for optimal detector per-

formance and suggests that temperature regulation can mitigate some of the variability in DCR readings.

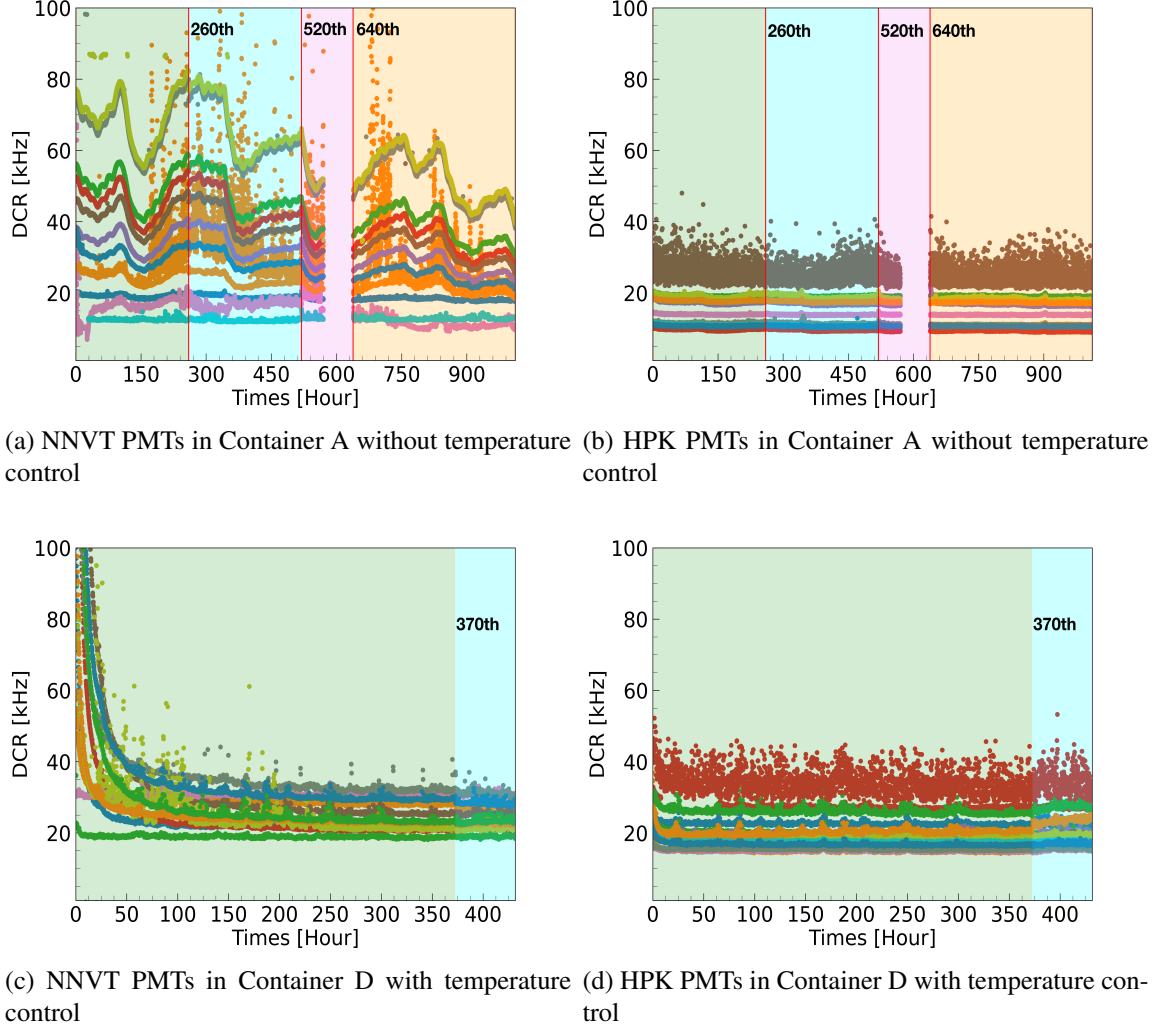


Figure 10: DCR monitoring of bare NNVT and HPK PMTs for a long-term in container A without temperature control and potted PMTs in container D with temperature control.

A successful monitoring of the long-term stability of 117 PMTs under various load conditions was performed, comprising of 73 tubes from NNVT and 44 from HPK. The test results of selected samples are illustrated in Figure 11. Among the monitored PMTs, the majority exhibited a stable and smooth distribution over time, as shown in Figure 11a. However, a subset of PMTs exhibited abnormal fluctuations during testing (see Figure 11b), where the DCR spiked to levels exceeding 100 kHz, surpassing our acceptance criteria. These anomalies could potentially be influenced by various hardware components, including electronics or the PMT units themselves, particularly during the occurrence of flashing PMTs.

To identify and diagnose potential issues stemming from connections or electronics, additional measurements were conducted. The first step involved swapping testing drawers and replacing

HV dividers, a straightforward approach to eliminate possible hardware problems. After these adjustments, some PMTs stabilized, as indicated by the cyan blue background in Figure 11b, and maintained this stability over an extended period. Conversely, several PMTs continued to exhibit instability, marked by a different background color in Figure 11c, despite the changes made. This persistent instability may indicate inherent issues with the PMTs themselves. Ultimately, approximately 7% of the long-term monitored PMTs displayed unstable DCR characteristics.

In summary, the abnormal jumps in DCR are detrimental to detector performance, as they can lead to false triggering and adversely affect energy measurements. While the underlying causes warrant further investigation beyond the container system's capabilities, a standalone inquiry will be addressed in subsequent discussions.

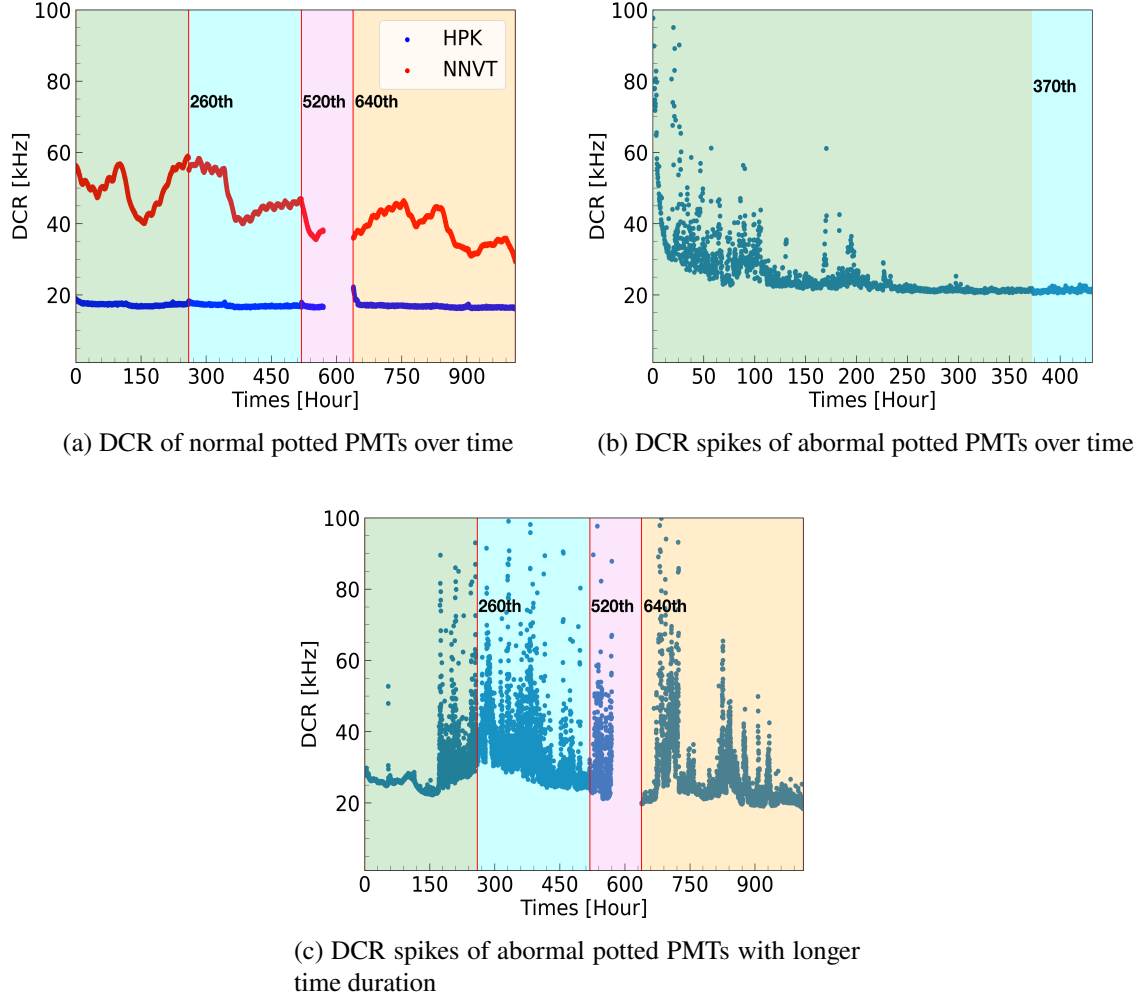


Figure 11: Long-term DCR monitoring: (a) DCR of normal potted PMTs over time (b) DCR spikes of abnormal NNVT potted PMTs over time, but after testing drawer swapping recovered as tagged by the cyan blue background. (c) abnormal NNVT DCR with jumps, but after testing drawer swapping, it is not recovered as tagged by the different color.

3.3.2 Short-term DCR Monitoring

During the mass testing of the JUNO bare PMTs, the DCR of each tested PMT was monitored at 30-minute intervals throughout a cooling period lasting 12 hours or longer, depending on their respective configurations. To minimize the effects of DCR shifts during the initial cooling phase, the evaluation of the monitored DCR was started only after the third hour. A focus was set specifically for significant DCR fluctuations, defined as increases exceeding 50 kHz or 50% compared to the previously recorded DCR point, as detailed in Section 3.3.1.

Figures 12a and 12b illustrate examples of the DCR behavior. Figure 12a features curves exhibiting normal and stable DCR characteristics, while Figure 12b shows a DCR curve with identified spikes.

The analysis found that approximately 20% of the tested PMTs experienced at least one jump in DCR, with about 0.2% exhibiting multiple jumps.

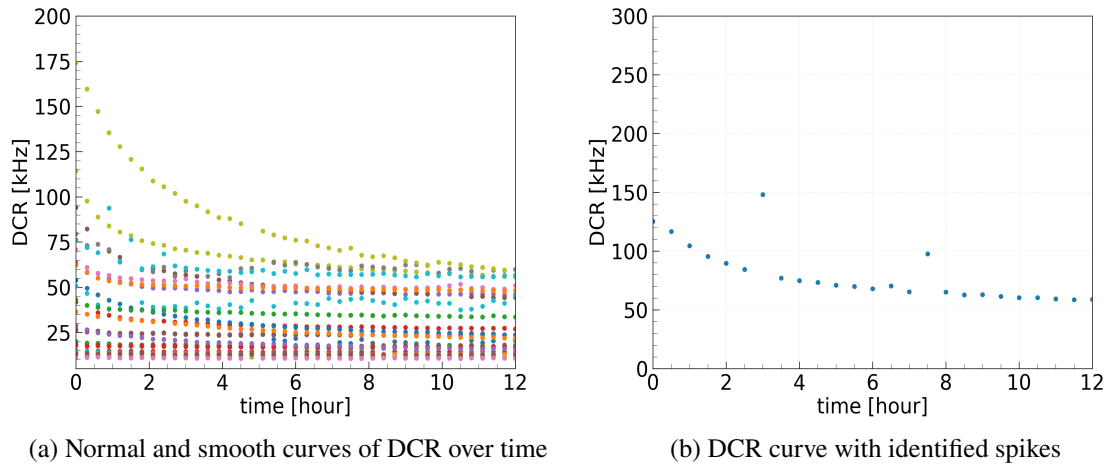


Figure 12: Monitored DCR of PMTs during their cooling time for the acceptance test: (a) normal DCR with smooth curve and (b) abnormal DCR curve with some spikes

3.4 Discussion

The cooling down time of the PMTs was found to be crucial for the DCR measurement. It is advisable to allow a longer cooling period of at least 50 hours for NNVT PMTs, while a minimum of 7 hours is sufficient for HPK PMTs. This extended cooling time ensures that DCR measurements achieve an uncertainty of less than 1 kHz. Notably, the DCR values observed during the JUNO PMT mass testing are slightly elevated compared to the anticipated baseline.

For accurate DCR measurements, it is recommended to control the temperature within ± 1 $^{\circ}$ C. This precision in temperature control is essential for achieving a DCR measurement accuracy of 1 kHz in the temperature range of 2 $^{\circ}$ C, which poses no challenge for the future JUNO detector operations.

Additionally, variations in DCR may be linked to several factors, including noise interference, cable and connector quality, electronic components, or even potential issues related to flashing

PMTs. These aspects necessitate further investigation to understand their impact on measurement consistency.

4 Possible Flasher Identification

PMT flasher is an important background/noise for the rare events' experiment [21, 22], which also can be identified by the monitored PMT DCR: the PMT itself and its neighbor PMTs. If the jumps originate from the PMTs or electronic sources, only the count rates for PMT random coincidences would significantly increase, without impacting other PMTs. Conversely, under sufficiently high emission intensity, all PMTs respond simultaneously, leading to concurrent increases in DCR across the board. To gain deeper insights into DCR jump from possible PMT flasher, a series of experiments was conducted at the Institute of High Energy Physics (IHEP) laboratory, as illustrated in Figures 13 and 15.

The setup configuration includes two 20-inch PMTs; NNVT and HPK tubes, and two 3-inch PMTs, produced by Hainan Zhanchuang Photonics Technology Co., Ltd (HZC), denoted as small PMT (sPMT). The 20-inch PMTs were positioned towards each other and two 3-inch PMTs were placed in between to enhance light collection and allow for potential flasher tagging. The two 20-inch PMTs operate at a gain of (1×10^7) and exhibited abnormal DCR behavior during the Pan-Asia test. Two 3-inch PMTs function at a lower gain of (3×10^6) . Notably, the threshold for the 3-inch PMTs is set at 0.25 photoelectrons (pe), while the DCR for the 20-inch PMTs is significantly higher, requiring a threshold of 10 pe to maintain a lower event rate. The distribution of parameters for all PMTs is summarized in Table 4.

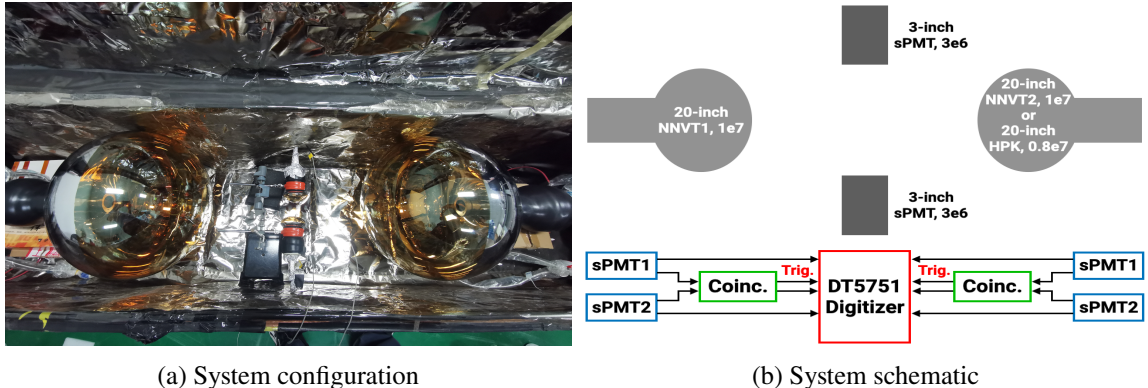


Figure 13: Experimental Setup

4.1 DCR Spike

With the setup shown in Figure 13, several notable DCR spikes can be identified in both 3-inch and 20-inch PMTs during the long-term monitoring as shown in Figure 14a (Two NNVT PMTs, NNVT+NNVT) and Figure 14b (One NNVT and one HPK PMTs, NNVT+HPK). In both cases, the instances of all four PMTs simultaneously experiencing DCR spikes within a monitoring duration of less than 300 hours are rare. An analysis of the monitoring results yields a random coincidence rate of 0.4×10^{-5} Hz for NNVT/NNVT and 3.6×10^{-5} Hz for NNVT/HPK, whereas the measured

Table 4: The PMT configuration setup, where the amplitude of a single p.e. for NNVT or HPK is around 8 mV, while it is around 20 mV for sPMT with an amplifier of 10 times

PMT	HV [V]	Threshold [pe]
NNVT1	1700	10
NNVT2	1850	10
HPK	2300	10
SPMT1	1180	0.25
SPMT2	1150	0.25

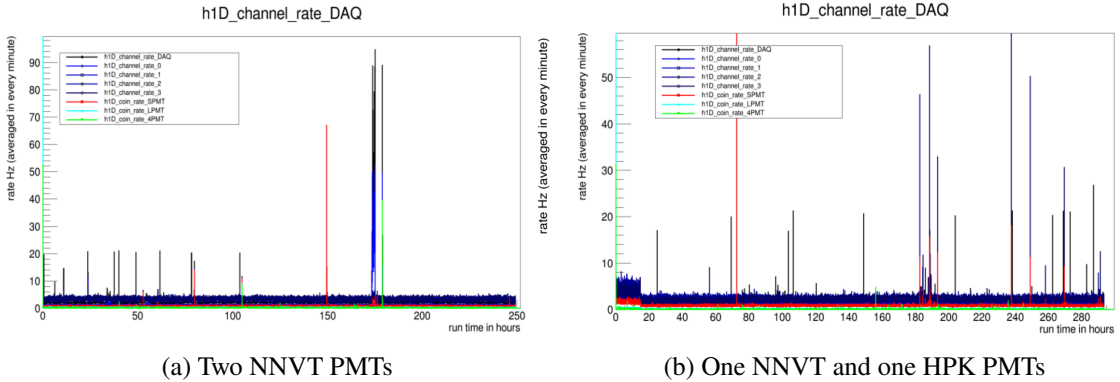


Figure 14: DCR monitoring in long term

coincidence rates exceed 0.5 Hz. This disparity primarily arises from the characteristics of the 20-inch PMT itself.

4.2 Investigation on DCR Spikes

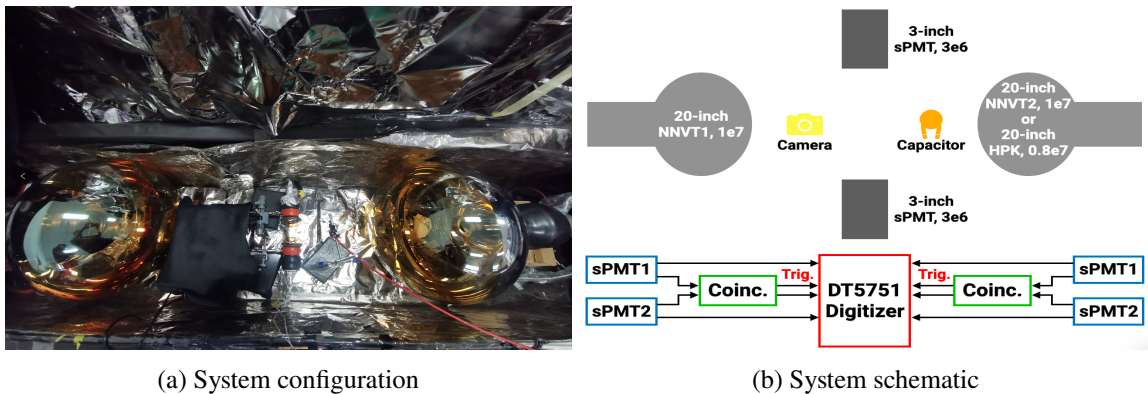


Figure 15: Experimental Setup for DCR spike with camera

A single photon sensitive camera (ORCA-Quest qCMOS C15550-20UP from Hamamatsu Photonics [37, 38]) is a useful tool to detect a weak light sources to investigate DCR spikes, where a voltage test and a capacitor test were designed in conjunction with the camera, as shown in Figure 15. In these tests, the camera was oriented towards a 20-inch PMT. In the voltage test,

we systematically increased the working voltage of PMT in increments of 100 V from a start of 1500 V and monitored the PMT's coincidence rates by a counter. Conversely, in the capacitor test, as illustrated in the diagram (Figure 15b), we introduced a capacitor chain and applied high voltage to make it spark. The breakdown of the capacitor generated flashes (artificial sparks), enabling the observation of the PMT's response through this test.

4.2.1 Tagging with Artificial Spark

The camera effectively captured the distinctive characteristics of the sparks produced by the capacitor at 2500 V. Figure 16 elucidates the specific events observed within the dark box. Additionally, Figure 16a visually represents the positioning of the capacitor under visible light. The subsequent three images document the sparking process as captured by the camera with an exposure time of 500 ms. Figure 16b depicts the state prior to the activation of the artificial spark. Following the breakdown of the capacitor, which resulted in the generation of sparks, the camera recorded the transient conditions within the dark box, as illustrated in Figure 16c. The photograph demonstrates a gradual weakening of the flash over the subsequent 500 ms, as evidenced in Figure 16d.

Simultaneously, the coincidence rate of the PMTs recorded by the counter is shown in Figure 17. During sparking, the rates of the PMTs exhibited distinct patterns, as indicated in the graph. It is clear that the rate increases rapidly when the spark occurs, demonstrating that the flash at this intensity can be simultaneously monitored by all PMTs. Notably, the rates of two 3-inch PMTs, along with their coincidence rate, showed a significant increasing. The rate of the 20-inch PMT also experienced a notable surge at the moment of ignition, although it remained static due to saturation effects. During the artificial spark, the system's coincidence rate reached saturation (approximately 1 kHz) and persisted for around 10 minutes. Following the spark, a gradual decrease in the coincidence rate was observed, in contrast to the rapid diminishing of the spark as documented by the camera. However, after the saturation effects subsided, the DCR of the 20-inch PMT declined. Concurrently, the accidental coincidence rate among all four PMTs exhibited a decreasing until its back to normal levels. These characteristic fluctuations in PMT coincidence counts are typical outcomes triggered by the externally applied ignition of the capacitor.

4.2.2 Check with Higher PMT HV

In this test, we investigate the intrinsic characteristics of the PMTs by increasing their working high voltage (HV) to enhance potential flasher. The study of flashers involves analyzing the coincidence rates at various operating voltages, as illustrated in Figure 18. The coincidence rate of the 20-inch PMTs increases with the rise in working voltage with a same threshold. Consequently, monitoring the coincidence rate of the smaller PMT can provide insights into the behavior of the larger PMT. The red line indicates the coincidence outcome for the 3-inch PMTs. Notably, when the working voltage of PMTs is raised by 500 V higher than the nominal HV of a gain of 1×10^7 , the event rate experiences a significant increase, while the event rates at other voltages remain stable. This observation suggests that under these conditions, the 3-inch PMT detects the PMT flashers emitted by the 20-inch PMT. In each configuration, the camera was used with a same configuration. However, it captured (one second exposure time) a possible flasher from the microchannel plate only at +500 V higher than the norminal HV, as shown in Figure 19.

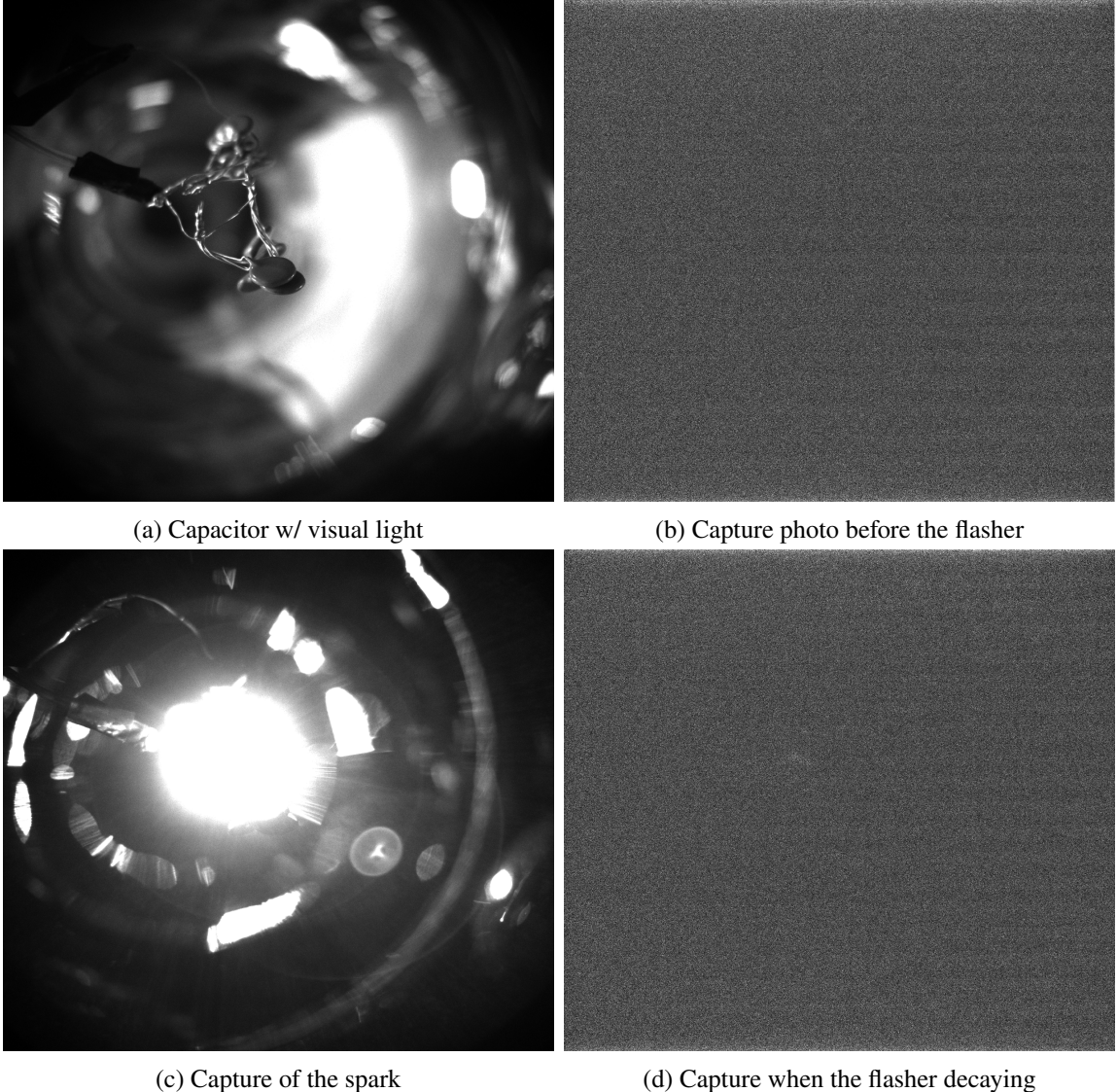


Figure 16: Visual capture of the artificial spark by capacitor

4.2.3 Discussion

With the artificial spark, the performance of the setup is checked: camera, PMT DCR spikes, PMT recovery, the coincidence among PMTs, which is valuable for better understanding the features of possible sparks. With the higher PMT working HV test to enhance the possible flashing of PMT inside, a possible flasher of NNVT PMT from the MCP is identified, and its image, recovery is monitored by the PMTs and the camera, which is valuable for further investigation.

5 Summary

This paper investigates the dark count rate (DCR) of the JUNO 20-inch PMTs occupied in a container system, focusing on the effects of cooling time, temperature, and long-term stability. It was found

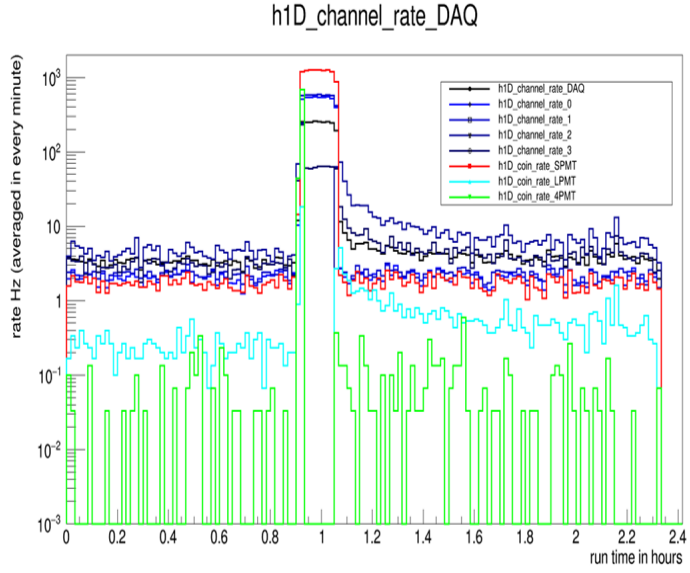


Figure 17: Flasher monitoring by PMT signal coincident rate

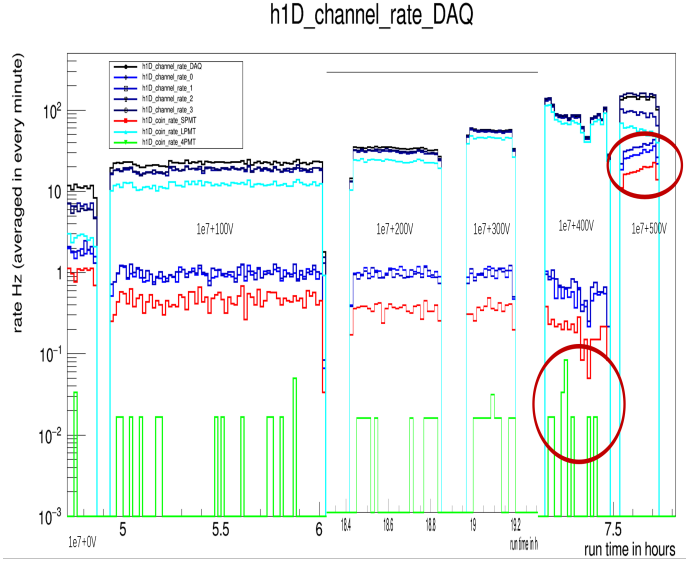
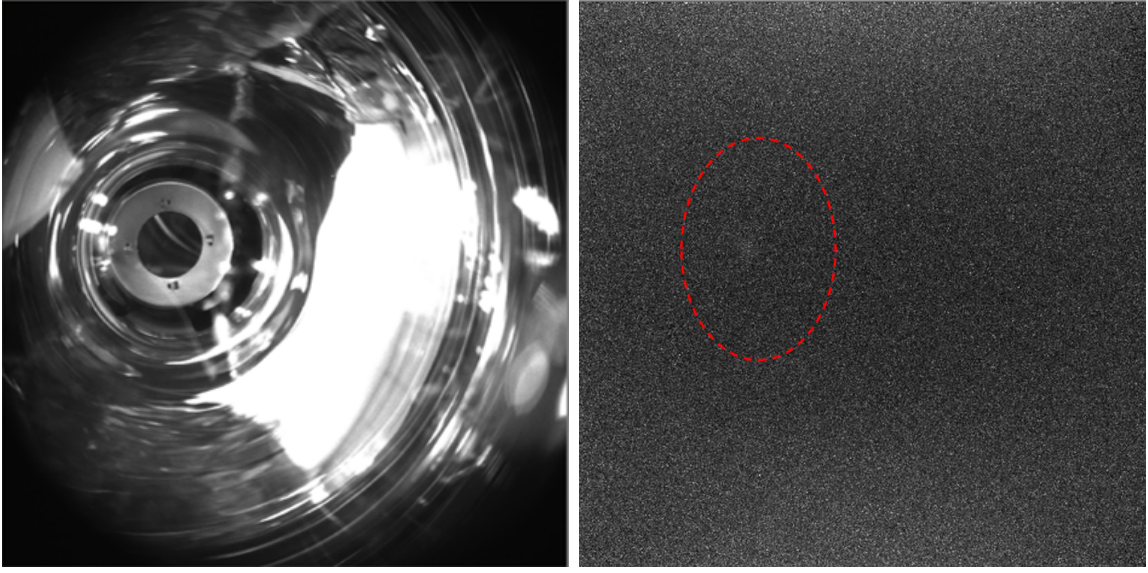


Figure 18: Monitored DCR during 20-inch PMT HV increasing in steps

that the DCR reduces during the cooling process of the bare PMTs. In addition an influence of both thermal effects and (previous) light exposure was found. Specifically, the NNVT PMTs exhibit a DCR decrease to approximately 56% of the measured value after a sufficient cooling time of 12 hours. In contrast, the HPK PMTs show a reduction to about 83% under the same conditions.

In terms of temperature effects on DCR variation, the HPK PMTs demonstrate a more consistent response to cooling and heating (within the temperature range of 14 °C to 28 °C) as well as at room temperature (ranging from 24 °C to 26 °C). For the HPK PMTs, DCR varies by about 2.0%/°C (or 0.55 kHz/°C) relative to the measurement at 21 °C.



(a) 20-inch NNVT PMT by the camera

(b) Possible candidate of flasher captured by the camera

Figure 19: Possible flasher monitoring by camera when the 20-inch PMT, applied +500 V additional to its gain 1×10^7 . These two photos are taken under the same position under the visible light and in dark.

Furthermore, the bare NNVT PMTs display a more pronounced temperature dependency, with a DCR variation of approximately $12.0\%/\text{ }^{\circ}\text{C}$ ($6\text{ kHz}/\text{ }^{\circ}\text{C}$) against the value at $21\text{ }^{\circ}\text{C}$, when observed between $14\text{ }^{\circ}\text{C}$ and $28\text{ }^{\circ}\text{C}$. For the potted NNVT PMTs, the DCR temperature coefficient is around $4.0\%/\text{ }^{\circ}\text{C}$ ($2\text{ kHz}/\text{ }^{\circ}\text{C}$) in the same range. This behavior suggests that the DCR becomes flatter with respect to temperature after the potting process for NNVT PMTs, particularly between $14\text{ }^{\circ}\text{C}$ and $21\text{ }^{\circ}\text{C}$. Notably, the trend remains consistent with room temperature monitoring, showing similar stability for both bare and potted PMTs in the range of $24\text{ }^{\circ}\text{C}$ to $26\text{ }^{\circ}\text{C}$.

During mass testing, approximately 20% of the PMTs exhibited abnormal DCR jumps at least once while monitoring cooling time, while long-term monitoring (involving around 110 PMTs) indicated abnormalities in about 7% of cases. These DCR jumps might be associated with noise, cables, connectors, and electronics components, as well as potential flashers of the PMTs, warranting further investigation.

Laboratory measurements on the NNVT PMTs with abnormal DCR revealed characteristics suggestive of artificial sparks with significant intensity, along with indications related to the microchannel Plate (MCP) when supplied with higher voltage. Photographic evidence captured instances of both potential flashers. Additionally, the time-dependence of DCR was monitored through the coincidence events of four PMTs.

Acknowledgments

This work was supported by the National Natural Science Foundation (NSFC) of China No. 11875282, the Strategic Priority Research Program of the Chinese Academy of Sciences, Grant

No. XDA10011100, the CAS Center for Excellence in Particle Physics, the Joint Institute of Nuclear Research (JINR), Russia and Lomonosov Moscow State University in Russia, the joint Russian Science Foundation (RSF), DFG (Deutsche Forschungsgemeinschaft). The authors acknowledge all colleagues from JUNO collaboration for operating the 20-inch PMT testing system.

References

- [1] F. An et al., *Neutrino physics with juno*, *Journal of Physics. G, Nuclear and Particle Physics* **43** (2016) .
- [2] J. collaboration, *JUNO physics and detector*, *Progress in Particle and Nuclear Physics* **123** (2022) 103927.
- [3] A. Abusleme et al., *The design and technology development of the juno central detector*, *Eur. Phys. J. Plus* **1128** (2024) .
- [4] JUNO collaboration, *Mass Testing and Characterization of 20-inch PMTs for JUNO*, *The European Physical Journal C* **82** (2022) 1168 [[2205.08629](https://arxiv.org/abs/2205.08629)].
- [5] C. Cao et al., *Mass production and characterization of 3-inch pmts for the juno experiment*, *Nuclear Instruments and Methods in Physics Research Section A: Accelerators, Spectrometers, Detectors and Associated Equipment* **1005** (2021) 165347.
- [6] F. Suekane, K. Collaboration et al., *Kamland*, *Progress in Particle and Nuclear Physics* **57** (2006) 106.
- [7] G. Alimonti, C. Arpesella, H. Back, M. Balata, D. Bartolomei, A. De Bellefon et al., *The borexino detector at the laboratori nazionali del gran sasso*, *Nuclear Instruments and Methods in Physics Research Section A: Accelerators, Spectrometers, Detectors and Associated Equipment* **600** (2009) 568.
- [8] J. Boger, R. Hahn, J. Rowley, A. Carter, B. Hollebone, D. Kessler et al., *The sudbury neutrino observatory*, *Nuclear Instruments and Methods in Physics Research Section A: Accelerators, Spectrometers, Detectors and Associated Equipment* **449** (2000) 172.
- [9] S. Fukuda, Y. Fukuda, T. Hayakawa, E. Ichihara, M. Ishitsuka, Y. Itow et al., *The super-kamiokande detector*, *Nuclear Instruments and Methods in Physics Research Section A: Accelerators, Spectrometers, Detectors and Associated Equipment* **501** (2003) 418.
- [10] F. An, J. Bai, A. Balantekin, H. Band, D. Beavis, W. Beriguete et al., *The detector system of the daya bay reactor neutrino experiment*, *Nuclear Instruments and Methods in Physics Research Section A: Accelerators, Spectrometers, Detectors and Associated Equipment* **811** (2016) 133.
- [11] H. Zhang, Z. Wang, F. jiao Luo, A. bo Yang, D. Wu, Y. Li et al., *Gain and charge response of 20" mcp and dynode pmts*, *Journal of Instrumentation* **16** (2021) .
- [12] Y. Maekawa, C. Fujisawa and Y. Nishimura, *Performance of 50 cm photomultiplier tube for hyper-kamiokande*, in *2021 IEEE Nuclear Science Symposium and Medical Imaging Conference (NSS/MIC)*, pp. 1–3, IEEE, 2021.
- [13] G. Kim, J. Lee and H. Kim, *Characterization of a 20-inch micro channel plate photomultiplier tube*, *New Physics: Sae Mulli* **72** (2022) 436.
- [14] Y. Chang et al., *The r&d of the 20in. mcp–pmts for juno*, *Nuclear Instruments and Methods in Physics Research Section A: Accelerators, Spectrometers, Detectors and Associated Equipment* **824** (2016) 143.

- [15] B. Wonsak, A. Tietzs, T. Sterr, T. Lachenmaier, N. Anfimov, D. Blum et al., *A container-based facility for testing 20'000 20-inch pmts for juno*, *Journal of Instrumentation* **16** (2021) T08001.
- [16] N. Anfimov, *Large photocathode 20-inch pmt testing methods for the juno experiment*, *Journal of Instrumentation* **12** (2017) C06017 .
- [17] J. Wang et al., *Database system for managing 20,000 20-inch pmts at juno*, *NUCL SCI TECH* **33** (2022) 24.
- [18] R. Zhao et al., *Afterpulse measurement of JUNO 20-inch PMTs*, arXiv: 2207.04995 (2022) [[2207.04995](https://arxiv.org/abs/2207.04995)].
- [19] C. Liu et al., *Check on the features of potted 20-inch PMTs with 1F3 electronics prototype at Pan-Asia*, arXiv: 2208.08264 (2022) [[2208.08264](https://arxiv.org/abs/2208.08264)].
- [20] J. Cao and K.-B. Luk, *An overview of the daya bay reactor neutrino experiment*, *Nuclear Physics B* **908** (2016) 62.
- [21] A. Yang, Z. Qin, Z. Wang, H. Chen, W. Wei, F. Luo et al., *Study and removal of the flash from the hv divider of the 20-inch pmt for juno*, *Journal of Instrumentation* **15** (2020) T04006.
- [22] S. Qian, F. Gao, L. Ma, Y. Zhu, S. Chen and P. Chen, *The study on the 20 inch pmt flasher signal*, *Journal of Instrumentation* **15** (2020) T06008.
- [23] Y. Zhang, Z. Wang, M. Li, Y. Zhang, Y. Wang, Z. Peng et al., *Study of 20-inch pmts dark count generated large pulses*, *Journal of Instrumentation* **17** (2022) P10048.
- [24] Y. Zhang, Z. Wang, M. Li, C. Liu, N. Rodphai, Y. Zhang et al., *Dark count of 20-inch pmts generated by natural radioactivity*, *Journal of Instrumentation* **19** (2024) P02026.
- [25] Hamamatsu Photonics K.K., “R12860 datasheet.”
- [26] N.N.V.T. Ltd., “Specification for GDB-6201 microchannel plate type photomultiplier PMT (in Chinese).”
- [27] L. Ren et al., *Study on the improvement of the 20-inch microchannel plate photomultiplier tubes for neutrino detector*, *Nucl. Instrum. Meth. A* **977** (2020) 164333.
- [28] L. Wen et al., *A quantitative approach to select PMTs for large detectors*, *Nucl. Instrum. Meth. A* **947** (2019) 162766 [[1903.12595](https://arxiv.org/abs/1903.12595)].
- [29] S. Zhang, J.-S. Li, Y.-J. Su, Y.-M. Zhang, Z.-Y. Li and Z.-Y. You, *A method for sharing dynamic geometry information in studies on liquid-based detectors*, *Nuclear Science and Techniques* **32** (2021) 1.
- [30] Y. Yu, H. Lv, K. Tariq, D. Liu, X. Sheng and C. Feng, *Study of the performance of photomultiplier tubes at high variable counting rates*, *Nuclear Instruments and Methods in Physics Research Section A: Accelerators, Spectrometers, Detectors and Associated Equipment* **1008** (2021) 165433.
- [31] M. Babicz et al., *Test and characterization of 400 hamamatsu r5912-mod photomultiplier tubes for the ICARUS t600 detector*, *Journal of Instrumentation* **13** (2018) P10030.
- [32] W. Chen et al., *Lock-in-photon-counting-based highly-sensitive and large-dynamic imaging system for continuous-wave diffuse optical tomography*, *Biomedical Optics Express* **7** (2016) 499.
- [33] H. Li, Q. Sen, Z. Ning, Y. Zhang, Q. Wu, L. Ma et al., *Study on the stability of 20 inch photomultiplier tubes based on microchannel plate*, *Journal of Instrumentation* **16** (2021) T06015.
- [34] S. Qian, F. Gao, L. Ma, Y. Zhu, S. Chen and P. Chen, *The study on the 20 inch pmt flasher signal*, *Journal of Instrumentation* **15** (2020) T06008.

- [35] A. Yang, Z. Qin, Z. Wang, H. Chen, W. Wei, F. Luo et al., *Study and removal of the flash from the hv divider of the 20-inch pmt for juno*, *Journal of Instrumentation* **15** (2020) T04006.
- [36] D. Liu, *Pmt evaluation for the daya bay neutrino experiment*, *IEEE Nuclear Science Symposium conference record. Nuclear Science Symposium* (2008) .
- [37] Z. Wang, M. Li, D. Wu et al., *Imaging of csi(tl) crystal event and double-slit young's interference by a single photon sensitive camera*, *Eur. Phys. J. Plus* **138** (2023) .
- [38] Z. Wang, M. Li, D. Wu, J. Liu, Y. Zhang, X. Meng et al., *Imaging of muon track in csi(tl) crystal with single photon sensitive camera*, *Journal of Instrumentation* **18** (2023) P09015.